COMPUTATIONAL ACOUSTICS - Volume 3
D. Lee, A. Cakmak, R. Vichnevetsky (Editors)
Elsevier Science Publishers B.V. (North-Holland)
IMACS, 1990

Three-dimensional sound propagation in shallow water including the effects of rough surfaces

Michael D. Collins and Stanley A. Chin-Bing
Naval Ocean Research and Development Activity
Stennis Space Center, MS 39529

Abstract

A three-dimensional parabolic equation (3DPE) that handles wide angles in the vertical, narrow angles in the azimuth, and rough ocean surfaces and bottoms is derived. The 3DPE is solved numerically using the method of alternating directions. Surface roughness is accounted for by a reflection coefficient that depends on grazing angle. Calculations are presented to illustrate the rough surface model and to demonstrate that azimuthal diffraction can be important in shallow water. The ability of the 3DPE to accurately handle azimuthal diffraction is demonstrated with a benchmark calculation. Algorithms for improving the efficiency of 3DPE models are discussed.

1. Introduction

The parabolic equation [1] (PE) method is a very useful model for underwater propagation calculations. For most applications of the PE, the domain is assumed to be cylindrically symmetric with smooth boundaries, and the two-dimensional PE (2DPE) is applied. Including the effects of three-dimensional variations and rough surfaces in the model would allow one to handle more realistic problems. The three-dimensional PE [2-5] (3DPE) has been derived for problems involving variations in both range and azimuth. For some problems, accurate results can be obtained for problems involving variations in azimuth by using the 2DPE in each direction of interest [3]. For such problems the azimuthal diffraction term in the 3DPE is apparently less important than the azimuthal refraction term. A 3DPE that handles wide-angle propagation in both depth and azimuth has been derived [4]. However, existing numerical solutions of this 3DPE are inefficient due to coupling between the depth and azimuth term. A 3DPE that handles wide angles in depth and narrow angles in azimuth can be solved very efficiently with the method of alternating directions [5]. Propagation in the ocean can be significantly affected by rough boundaries. [6] An efficient approach for modeling rough ocean surfaces and bottoms is to assume that the net result of the roughness is an energy loss that depends on grazing angle [7,8].

In this paper, a 3DPE is derived that handles wide angles in depth and narrow angles in azimuth and includes rough boundaries. Rough ocean surfaces and bottoms are handled approximately by assuming a reflection coefficient at the ocean surface that depends on grazing angle and transforming this into a homogeneous boundary condition that is easily incorporated into the numerical solution of the 3PDE. The reflection coefficient is allowed to vary in both range and azimuth. Calculations are presented to illustrate the rough surface PE and to demonstrate that the 2DPE can not handle some shallow-water propagation problems. Efficient algorithms for the numerical solution of the 3DPE are discussed and illustrated with examples. The ability of the 3DPE to accurately handle azimuthal diffraction is demonstrated with a benchmark calculation.

2. The three-dimensional parabolic equation

We work in cylindrical coordinates with z being the depth below the ocean surface, θ being the azimuth angle, and r being the horizontal distance (range) from a time-harmonic point source of circular frequency ω. For now, we assume that the complex wavenumber $K = k + i\eta\beta \mid k \mid$ and the density ρ depend only on z, where $k = \omega/c, \beta$ is the attenuation in decibels per wavelength, c is the sound speed, and $\eta = (40\pi \log_{10} e)^{-1}$. We define the reference sound speed c_0 and reference wavenumber $k_0 = \omega/c_0$. Cylindrical spreading is handled by removing the factor $r^{-\frac{1}{2}}$ from the complex pressure P.

For $kr >> 1, P$ is assumed to satisfy the farfield equation

$$\frac{\partial^2 P}{\partial z^2} - \frac{1}{\rho}\frac{\partial \rho}{\partial z}\frac{\partial P}{\partial z} + \frac{\partial^2 P}{\partial r^2} + \frac{1}{r^2}\frac{\partial^2 P}{\partial \theta^2} + K^2 P = 0. \tag{2.1}$$

Since r^{-2} may be assumed to commute with $\partial/\partial r$ in the farfield, we obtain the following factorization for the outgoing solution

$$\frac{\partial P}{\partial r} = ik_0 \sqrt{1 + \frac{K^2 - k_0^2 + \frac{\partial^2}{\partial z^2} - \frac{1}{\rho}\frac{\partial \rho}{\partial z}\frac{\partial}{\partial z} + \frac{1}{r^2}\frac{\partial^2}{\partial \theta^2}}{k_0^2}}\, P. \tag{2.2}$$

We define the operators

$$X = k_o^{-2}\left(K^2 - k_0^2 + \frac{\partial^2}{\partial z^2} - \frac{1}{\rho}\frac{\partial \rho}{\partial z}\frac{\partial}{\partial z}\right) \tag{2.3}$$

$$Y = \frac{1}{k_0^2 r^2}\frac{\partial^2}{\partial \theta^2} \tag{2.4}$$

and assume that $\mid YP \mid << \mid XP \mid$. For the square root in Eq. (2.2), we use the approximation

$$\sqrt{1 + X + Y} = 1 + \frac{2X}{4 + X} + \frac{1}{2}Y + O(X^3, XY) \tag{2.5}$$

and remove the plane wave factor $\exp(ik_o r)$ from P to obtain the 3DPE

$$\frac{\partial P}{\partial r} = \frac{2ik_0\left(K^2 - k_0^2 + \frac{\partial^2}{\partial z^2} - \frac{1}{\rho}\frac{\partial \rho}{\partial z}\frac{\partial}{\partial z}\right)}{3k_0^2 + K^2 + \frac{\partial^2}{\partial z^2} - \frac{1}{\rho}\frac{\partial \rho}{\partial z}\frac{\partial}{\partial z}} P + \frac{i}{2k_0 r^2}\frac{\partial^2 P}{\partial \theta^2}. \tag{2.6}$$

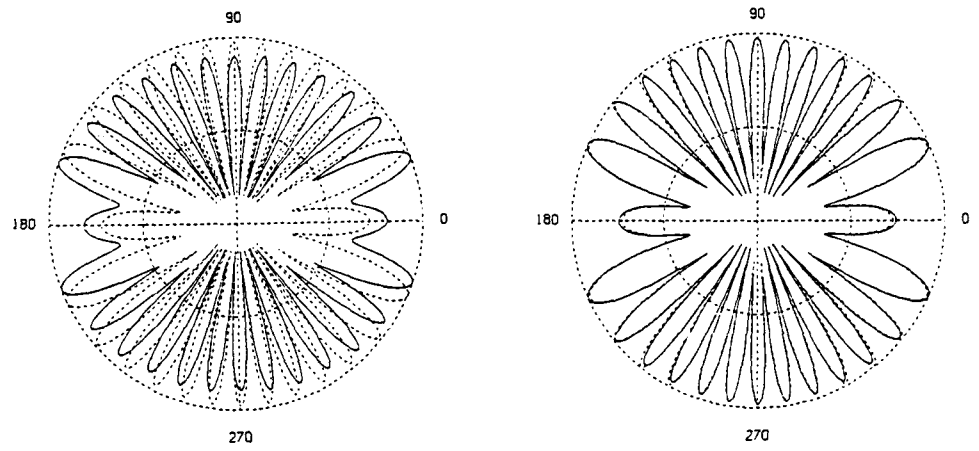

Figure 1: The modal radiation patterns for P_h at $r = 300$m (dashed curves) and for P (solid curves) at (a) $r = 150$m and (b) $r = 300$m.

Equation (2.6), which reduces to the wide-angle 2DPE [9] for two-dimensional problems, is a valid leading-order solution to problems in which K and ρ depend on r and θ as a perturbation. An analogous approach based on Eq. (2.5) has been used to derive a wide-angle time-domain PE for shallow water. [10]

We solve the 3DPE numerically with the method of alternating directions, [11] which requires numerical methods for each of the following

$$\frac{\partial P}{\partial r} = \frac{2ik_0\left(K^2 - k_0^2 + \frac{\partial^2}{\partial z^2} - \frac{1}{\rho}\frac{\partial \rho}{\partial z}\frac{\partial}{\partial z}\right)}{3k_0^2 + K^2 + \frac{\partial^2}{\partial z^2} - \frac{1}{\rho}\frac{\partial \rho}{\partial z}\frac{\partial}{\partial z}} P \tag{2.7}$$

$$\frac{\partial P}{\partial r} = \frac{i}{2k_0 r^2}\frac{\partial^2 P}{\partial \theta^2}. \tag{2.8}$$

Equation (2.7) is the wide-angle 2DPE and can be solved with the numerical methods described in Ref. 10. Equation (2.8) can be solved with centered differences in θ with Crank-Nicolson integration in r. The matrices involved have three diagonals and entries in the upper right and lower left corners for the continuity condition

$$P\,|_{\theta=0} = P\,|_{\theta=2\pi}\,. \tag{2.9}$$

To show that the 3DPE accurately handles azimuthal diffraction (i.e. the effect of the θ-term in the 3DPE), we consider a dipole source with a horizontal polar axis. In an ocean of depth 300m with $c = 1500$m/s, we place two 50Hz sources in phase 200m apart both at $z = 25$m. The point

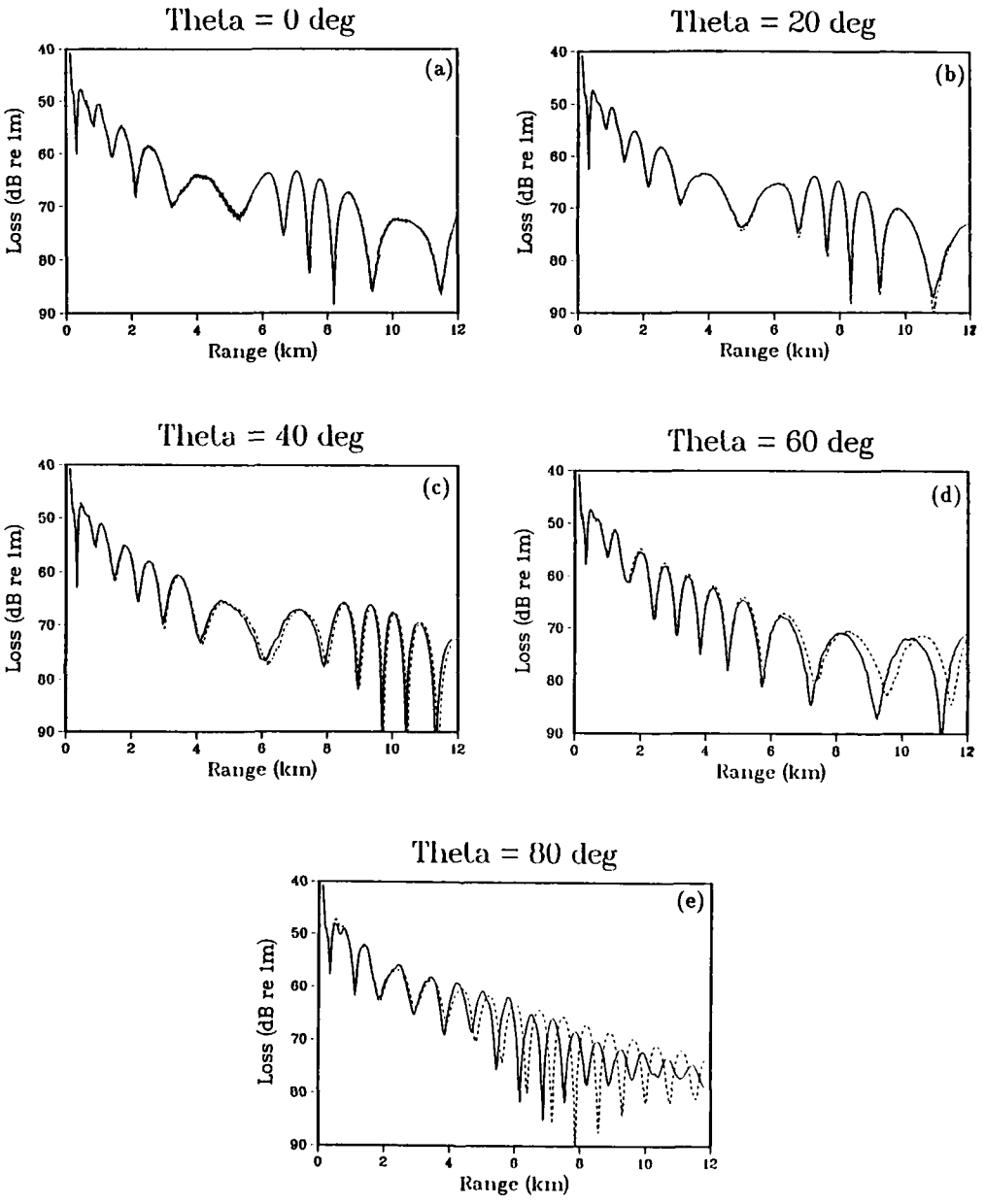

Figure 2: Transmission loss at z = 30m in an ocean with a corrugated bottom generated with the 3DPE (solid curves) and with the 2DPE (dashed curves) for (a) $\theta = 0°$, (b) $\theta = 20°$, (c) $\theta = 40°$, (d) $\theta = 60°$, (e) $\theta = 80°$, (Figure 2. cont'd on next page)

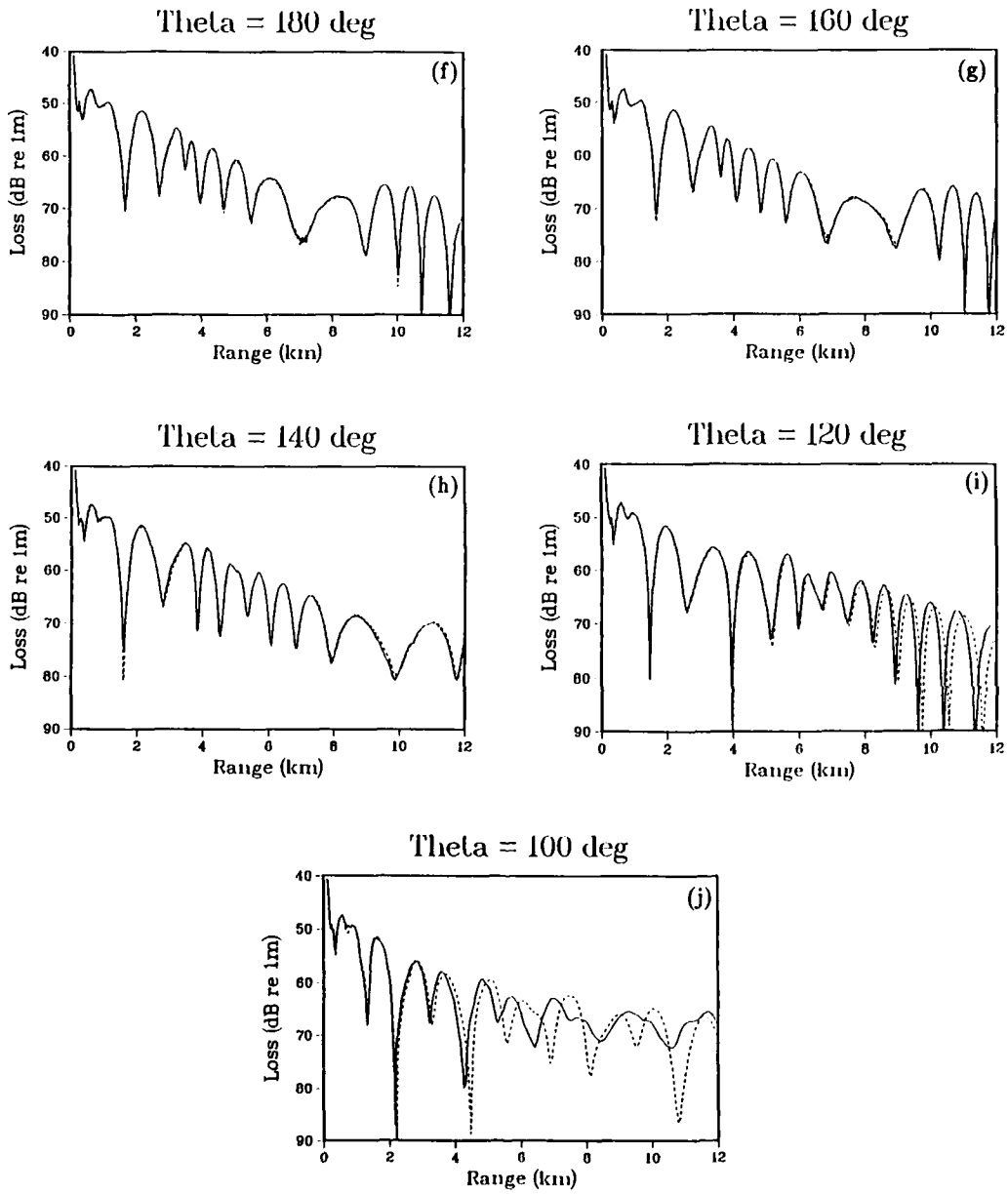

Figure 2 cont'd: Transmission loss at z = 30m in an ocean with a corrugated bottom generated with the 3DPE (solid curves) and with the 2DPE (dashed curves) for (f) $\theta = 100°$, (g) $\theta = 120°$, (h) $\theta = 140°$, (i) $\theta = 160°$, (j) $\theta = 180°$.

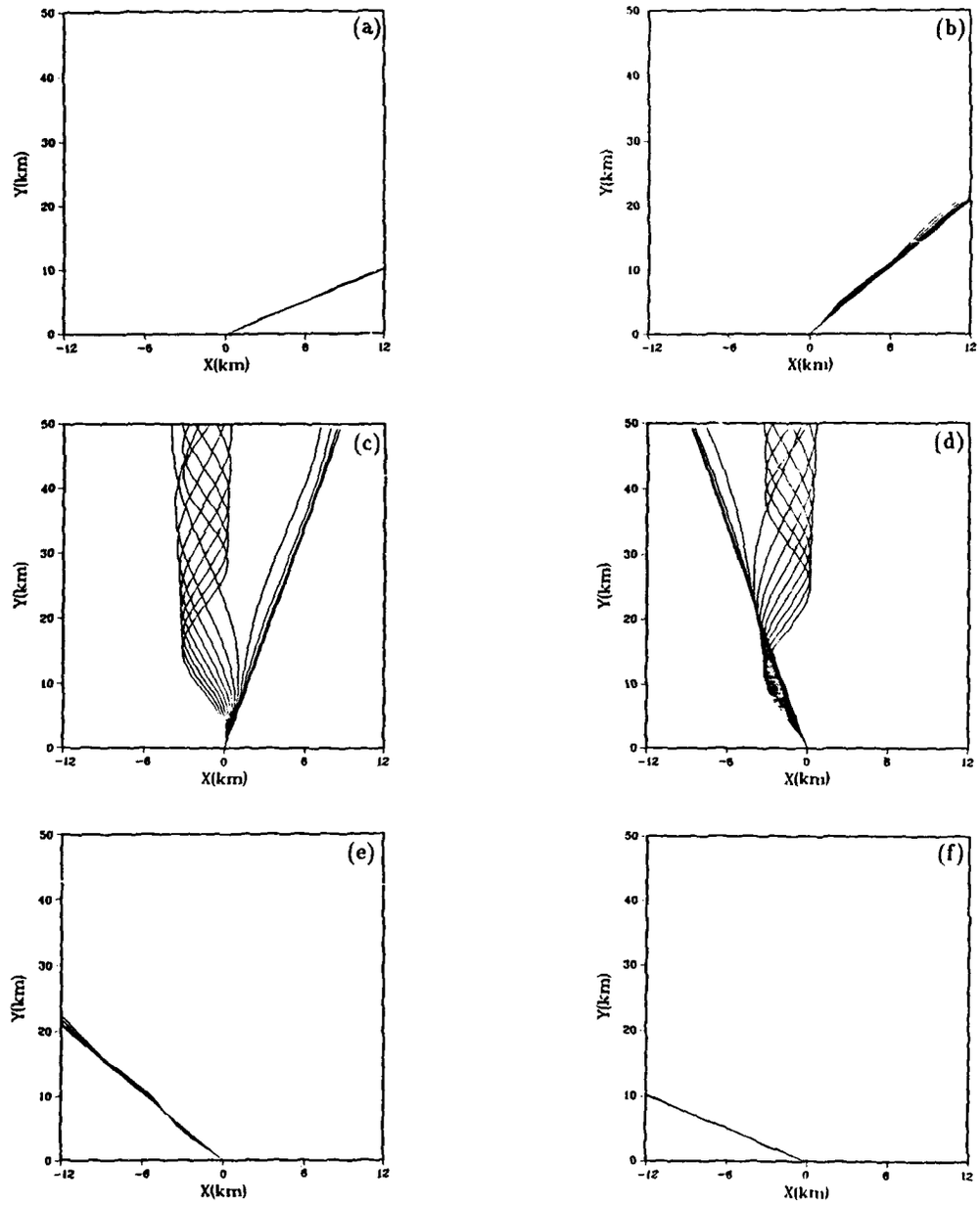

Figure 3: Rays traced from the origin in an ocean with a corrugated bottom for (a) $\theta = 40°$, (b) $\theta = 60°$, (c) $\theta = 80°$, (d) $\theta = 100°$, (e) $\theta = 120°$, (f) $\theta = 140°$.

midway between the sources is $r = 0$. In the sediment, c = 1600m/s, ρ = 1.5g/cm, and β = 0.5. The homogeneous half-space field [12]

$$P_h = \frac{1}{d_-} \exp(ik_0 d_-) - \frac{1}{d_+} \exp(ik_o d_+) \tag{2.10}$$

$$d_\pm^2 = r^2 + (z \pm z_0)^2 \tag{2.11}$$

is used as an initial condition at r = 150m, and the 3DPE is applied to march the field out to r = 300m. The modal radiation patterns [13] $20\log_{10} |< P, \psi_1 >|$ and $20\log_{10} |< P_h, \psi_1 >|$ appear in Figure 1, where ψ_1 is the first waveguide normal mode and $<,>$ is the inner product associated with the depth operator of Eq. (2.1). The half-space radiation pattern evolves substantially over 150m < r < 300m, and the radiation patterns are in excellent agreement at r = 300m.

To demonstrate that azimuthal diffraction can be important, we consider a 25Hz source at z = 25m in an ocean of depth

$$d = \left[3 - \sin\left(\frac{2\pi x}{6\text{km}}\right)\right] 50\text{m}, \tag{2.12}$$

which depends only on the Cartesian coordinate $x = r\cos\theta$. The maximum slope of the ocean bottom is about 3°. In the water column, we take c = 1500m/s. In the sediment, c = 1700m/s, ρ = 1.5g/cm^3, and β = 0.5. The domain is truncated at z = 600m, and the attenuation is increased linearly to 20 in the lower 100m of the domain to prevent reflections. The grid spacings are Δr = 5m, Δz = 1m, and $\Delta\theta$ = 0.25°. Transmission loss computed with the 2PDE and the 3DPE appears in Figure 2. We observe that the solutions are in good agreement for θ near 0° and 180°. Near 90°, however, there is a large difference between the solutions because energy gets trapped in the deep parts of the corrugated bottom and channeled in the y-direction. Similar effects should be important for many realistic shallow-water problems.

The three-dimensional behavior we have observed can also be illustrated with ray tracing. The grazing angle ϕ of a ray is defined to be the angle the ray makes with the ocean surface. Rays are traced from the origin for $\phi = 2n°$ for $1 \le n \le 15$. Rays that encounter the ocean bottom reflect (terminate) if incident within (beyond) the critical angle. Projections of the ray paths onto the ocean surface appear in Figure 3. Ray channeling is significant only for $60° \le \theta \le 120°$, which is consistent with the 3DPE results. For the case of $\theta = 80°$, the rays in Figure 3 are trapped in the channel for $5 \le n \le 13$.

3. Rough surface modeling

In the farfield, we consider the plane wave

$$P_i = \exp[ik(r\cos\phi - z\sin\phi)] \tag{3.1}$$

incident upon a rough ocean surface. As in Ref. 7, we assume that the scattered field is given by

$$P_s = -R(\phi) \exp\left[ik(r\cos\phi + z\sin\phi)\right], \tag{3.2}$$

where R is the reflection coefficient. Since a rough ocean surface results in variations in path lengths and thus phase distortions, we allow R to be complex. Since a rough surface behaves like a smooth reflector at small grazing angles, [14] $R(0) = 1$. Since $|\phi| << 1$ for rays in the farfield, we may assume

$$R \sim 1 + \alpha_1\phi + \alpha_2\phi^2 + ... \tag{3.3}$$

We use Eqs. (3.1), (3.2), and (3.3) to determine β_j such that the following expression for the total field $P = P_i + P_s$ is correct to the appropriate order in ϕ at $z = 0$:

$$\beta_1 P + \beta_2 \frac{\partial P}{\partial z} + \beta_3 \frac{\partial^2 P}{\partial z^2} + \frac{\partial}{\partial r}\left(\beta_4 P + \beta_5 \frac{\partial P}{\partial z} + \beta_6 \frac{\partial^2 P}{\partial z^2}\right) = 0. \tag{3.4}$$

To avoid a degenerate solution, it is necessary to assume that some of the coefficients in Eq. (3.4) vanish. For the case $\beta_j = 0$ for $j > 2$, we obtain

$$2kP + i\alpha_1 \frac{\partial P}{\partial z} = 0. \tag{3.5}$$

This approach can also be applied for the cases $\beta_1 = \beta_2 = \beta_6 = 0$ (wide angle) and $\beta_1 = \beta_2 = 0$ (very wide angle) for better accuracy. To model rough surfaces with the 3DPE, we replace the pressure release boundary condition $P = 0$ that is usually used in PE models with Eq. (3.4). This approach is easily implemented numerically into Eq. (2.7). A nonphysical depth grid point is introduced at $z = -\Delta z$ and Eq. (3.4) is assigned to this point. Equation (3.4) is discretized using centered differences in both r and z, and Eq. (2.7) is assigned to each of the physical depth grid points $z \geq 0$ and discretized with Galerkin's method and Crank-Nicolson integration as described in Ref. 10.

The plane wave reflection coefficient can be approximately introduced into the normal mode solution [15]

$$P = \sum_j a_j \psi_j(z) \exp\left(ik_j r\right) \tag{3.6}$$

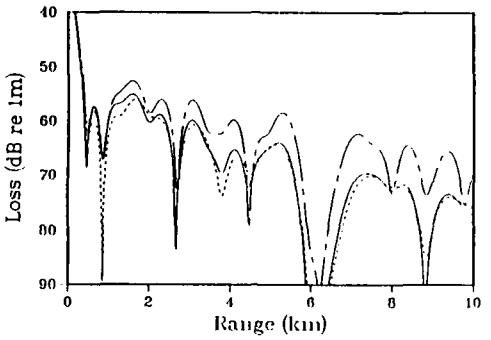

Figure 4: Transmission loss at z = 25m in an ocean with a rough surface. The PE solution (solid curve) versus the normal mode solution (dashed curve). The broken curve is the smooth surface PE solution.

as a perturbation, where a_j are constants, ψ_j are modes, and k_j are complex eigenvalues. We assume that the leading-order effect of this perturbation is to increase loss. For simplicity, c is taken to be constant in the water column. The number of surface bounces that a mode propagating at the angle ϕ_j experiences over the range r in an ocean of depth d is $r\tan\phi_j/2d$. Thus a leading-order rough surface normal mode solution is

$$P = \sum_j a_j \psi_j(z) R(\phi_j)^{\,r\tan\phi_j/2d} \exp(ik_j r). \tag{3.7}$$

Equation (3.7) is similar to the rough surface normal mode model of Ref. 8, which was used to model both rough ocean surfaces and rough ocean bottoms. Thus the rough surface 3DPE should be valid even for modeling rough ocean bottoms. Since the boundary condition is applied at the ocean surface, this is not obvious from the derivation.

To test the rough surface PE, we consider a stratified ocean of depth 200m in which c = 1500m/s. We take α_1 = -1 and place a 50Hz source at z = 25m. In the ocean bottom, c = 1600m/s, ρ = 1.5g/cm^3, and β = 0.5. Transmission loss computed with Eq. (3.7) and with the rough and smooth surface 2DPE models appears in Figure 4. The rough surface solution exhibits more loss than the smooth surface solution. Furthermore, the rough surface 2DPE and normal mode solutions are in good agreement. The agreement is not perfect, however, because the normal mode model was derived from the PE model by approximation. Since α_1 was taken to be real, the minima of the transmission loss curves are coincident for the smooth surface and rough surface results.

To illustrate the rough surface PE model in range-dependent domains, we consider the cylindrically symmetric rough bottom problem of Ref. 6. The ocean bottom is smooth for r < 5km. In the rough bottom region 5km < r < r_M, $d(r)$ is a square wave with d = 90m at the 50m wide minima and d = 100m at the 50m wide maxima. The cases r_M = 10km and r_M = ∞ are considered. A 25Hz source is placed at z = 18m. In the bottom, c = 1704.5m/s, ρ = 2.5g/cm^3, and β = 0.5. It is clear from Figures 4 and 5 of Ref. 6 that the rough bottom alters both phases and amplitude as

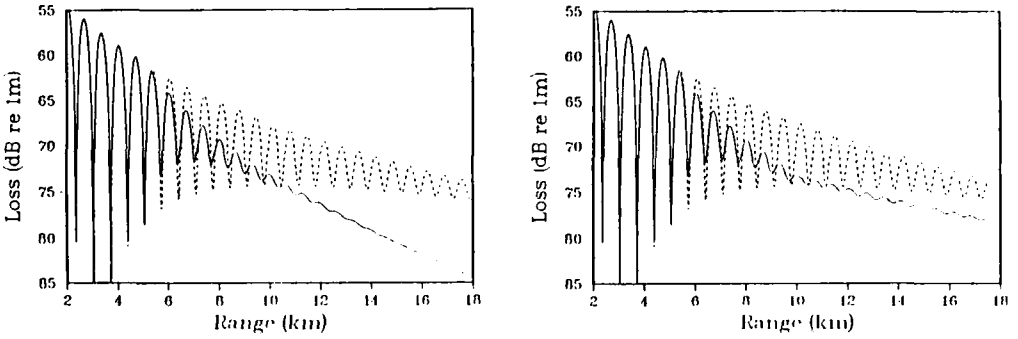

Figure 5: Transmission loss at $z = 50$m in an ocean with a rough surface for (a) $r > 5$km and (b) for 5km $< r <$ 10km. The solid curve is the rough surface PE solution. The dashed curve is the smooth surface PE solution.

the minima of the transmission loss curves for the smooth and rough cases do not coincide. Thus R is complex for this problem. Transmission loss for the smooth surface PE solution and the rough surface PE solution for $\alpha_1 = -\frac{3}{5}\exp(2\pi i/9)$ appear in Figure 5. The discontinuities in α_1 were handled with linear variations over short ranges. The rough surface PE solutions are similar to the normal mode solutions in Ref. 6.

4. Efficient PE algorithms

Finite difference solutions of a 2DPE involve a system of linear equations involving a tridiagonal matrix. It is natural to solve this system using Gaussian elimination from the ocean surface down to the bottom of the grid. Since the system is solved repeatedly as the solution is marched in range, a great deal of efficiency can be gained by decomposing the matrix into upper and lower triangular matrices. An efficient 2DPE code for range-independent problems would have FORTRAN loops in the tridiagonal solver subroutine similar to:

```
      DO 1   I = 2, N
      U(I) = A(I)*U(I) + B(I)*U(I-1)
1     CONTINUE
      DO 2    I = N-1, 1, -1
      U(I) = U(I) + C(I)*U(I +1)
2     CONTINUE
```

The first loop corresponds to downward elimination. The second loop corresponds to back substitution.

The diagonals A, B, and C are determined from the triangular decomposition and stored. Since computers perform multiplication significantly faster than division, it is better to store these constants as factors rather than divisors as we illustrate with a benchmark problem. [16,17] We consider a range-dependent problem for which the ocean depth decreases linearly from 200m at r = 0 to zero at r = 4km. A 25Hz source is placed at z = 100m in an ocean in which c = 1500m/s. In the bottom, c = 1700m/s, ρ = 1.5g/cm^3, and β =0.5. We truncate the domain at z = 2km and take Δr = 5m and Δz = 0.5m. These parameters were used in Ref. 16 to solve this problem using the PE code IFD, [18,19] which performs division in the loops. The run time reported in Ref. 16 was 7min on an FPS-164 computer. Using Gaussian elimination with the PE code FEPE, [20] which does not have division in the solver loops, the run time is 2min on an FPS-164.

Gaussian elimination is not the most efficient algorithm for problems involving range-dependent ocean depth. As depth varies, it is necessary to modify the entries of the matrix rows corresponding to the vicinity of the ocean bottom interface. Thus it is necessary to repeat downward elimination below the interface. A more efficient approach is to eliminate the entries below the main diagonal from the ocean surface down to the ocean bottom and to eliminate the entries above the main diagonal from the bottom of the domain up to the ocean bottom. With this approach, it is necessary to repeat the elimination process only for the rows near the ocean bottom as depth varies, and run time is essentially independent of bathymetry variations. Furthermore, this algorithm is vectorizable and may improve run times by up to a factor of two on a vector machine. Using this approach in FEPE, the run time for the benchmark problem is 1min on an FPS-164. For rough surfaces in which the β_j require frequent updates, it may be useful to perform Gaussian elimination from the bottom of the grid up to the ocean surface.

5. Conclusion

A 3DPE that handles wide angles in depth and narrow angels in azimuth and rough surfaces has been derived and solved numerically using alternating directions. Surface roughness was handled by assuming a reflection coefficient that depends on grazing angle and implemented into the 3DPE as a homogeneous boundary condition. The accuracy of the 3DPE was tested with a benchmark calculation. Calculations were presented to illustrate the rough surface model and to demonstrate that azimuthal diffraction can be important in shallow water. Efficient PE algorithms have been considered.

Acknowledgments

This work was supported by the Office of Naval Research and the Naval Ocean Research and Development Activity.

References

[1] Tappert, F.D, "The Parabolic Approximation Method," in *Wave Propagation and Underwater Acoustics*, edited by J.B. Keller and J.S. Papadakis, Lecture Notes in Physics, Vol. 70, Springer, New York, 1977.

[2] Baer, R.N., "Propagation through a Three-Dimensional Eddy Including Effects on an Array," *J. Acoust. Soc. Am.*, 1981, 69, 70-75.

[3] Perkins, J.S. and Baer, R.N., "An Approximation to the Three-Dimensional Parabolic-Equation Method for Acoustic Propagation," *J. Acoust. Soc. Am.*, 1982, 72, 515-522.

[4] Siegmann, W.L., Kriegsmann, G.A., and Lee, D., "A Wide-Angle Three-Dimensional Parabolic Wave Equation," *J. Acoust. Soc. Am.*, 1985, 78, 659-664.

[5] Lee, D., Saad, Y., and Schultz, M.H., "An Efficient Method for Solving the Three-Dimensional Wide Angle Wave Equation," Yale Univ. Res. Rep. YALE/DCS/RR-463.

[6] Evans, R.B. and Gilbert, K.E., "The Periodic Extension of Stepwise Coupled Modes," *J. Acoust. Soc. Am.*, 1985, 77, 983-988.

[7] Bucker, H.P., "Sound Propagation in a Channel with Lossy Boundaries," *J. Acoust. Soc. Am.*, 1970, 48, 1187-1194.

[8] Kuperman, W.A. and Ingenito, F., "Attenuation of the Coherent Component of Sound Propagating in Shallow Water with Rough Boundaries," *J. Acoust. Soc. Am.*, 1977, 61, 1178-1187.

[9] Claerbout, J.F., *Fundamentals of Geophysical Data Processing*, McGraw-Hill, New York, 1976, 206-207.

[10] Collins, M.D., "The Time-Domain Solution of the Wide-Angle Parabolic Equation Including the Effects of Sediment Dispersion," *J. Acoust. Soc. Am.*, 1988, 84, 2114-2125.

[11] Mitchell, A.R. and Griffiths, D.F., *The Finite Difference Method in Partial Differential Equations*, Wiley, New York, 1980, 59-70.

[12] Collins, M.D., "A Nearfield Asymptotic Analysis for Underwater Acoustics," *J. Acoust. Soc. Am.*, 1989, 85, 1107-1114.

[13] Collins, M.D. and Werby, M.F., "A Parabolic Equation Model for Scattering in the Ocean," *J. Acoust. Soc. Am.*, 1989, 85, 1895-1902.

[14] Tolstoy, I. and Clay, C.S., *Ocean Acoustics: Theory and Experiment in Underwater Sound*, American Institute of Physics, New York, 1987, 193.

[15] Evans, R.B., "A Coupled Mode Solution for Acoustic Propagation in a Waveguide with Stepwise Depth Variations of a Penetrable Bottom," *J. Acoust. Soc. Am.*, 1983, 74, 188-195.

[16] Jensen, F.B. and Ferla, C.M., "Numerical Solutions of Range-Dependent Benchmark Problems in Ocean Acoustics," *J. Acoust. Soc. Am.*, to appear.

[17] Collins, M.D., "Benchmark Calculations for Higher-Order Parabolic Equations," *J. Acoust. Soc. Am.*, to appear.

[18] Lee, D., Botseas, G., and Papadakis, J.S., "Finite-Difference Solution to the Parabolic Wave Equation," *J. Acoust. Soc. Am.*, 1981, 70, 795-800.

[19] Botseas, G., Lee, D., and Gilbert, K.E., "IFD: Wide-Angle Capability," NUSC Tech. Rep. 6905, 1983.

[20] Collins, M.D., "FEPE User's Guide," NORDA Tech. Note 365, 1988.

REPORT DOCUMENTATION PAGE

Form Approved
OMB No. 0704-0188

1. Agency Use Only *(Leave blank).*	2. Report Date.	3. Report Type and Dates Covered.
	1990	Proceedings

4. Title and Subtitle.
Three-dimensional sound propagation in shallow water including the effects of rough surfaces

5. Funding Numbers.
Program Element No. 61153N
Project No. 03205
Task No. 330
Accession No. DN257033

6. Author(s).
Michael D. Collins and Stanley A. Chin-Bing

7. Performing Organization Name(s) and Address(es).
Naval Oceanographic and Atmospheric Research Laboratory*
Stennis Space Center, MS 39529-5004

8. Performing Organization Report Number.
PR 89:033:220

9. Sponsoring/Monitoring Agency Name(s) and Address(es).
Naval Oceanographic and Atmospheric Research Laboratory*
Stennis Space Center, MS 39529-5004

10. Sponsoring/Monitoring Agency Report Number.
PR 89:033:220

11. Supplementary Notes.
*Formerly Naval Ocean Research and Development Activity

12a. Distribution/Availability Statement.
Approved for public release; distribution is unlimited.

12b. Distribution Code.

13. Abstract *(Maximum 200 words).*
A three-dimensional parabolic equation (3DPE) that handles wide angles in the vertical, narrow angles in the azimuth, and rough ocean surfaces and bottoms is derived. The 3DPE is solved numerically using the method of alternating directions. Surface roughness is accounted for by a reflection coefficient that depends on grazing angle. calculations are presented to illustrate the rough surface model and to demonstrate that azimuthal diffraction can be important in shallow water. The ability of the 3DPE to accurately handle azimuthal diffraction is demonstrated with a benchmark calculation. Algorithms for improving the efficiency of 3DPE models are discussed.

14. Subject Terms.
(U) Acoustic Waves; (U) Elastic Waves; (U) Seismic Waves

15. Number of Pages.
19

16. Price Code.

17. Security Classification of Report.	18. Security Classification of This Page.	19. Security Classification of Abstract.	20. Limitation of Abstract.
Unclassified	Unclassified	Unclassified	SAR